Chemical Engineering Journal 148 (2009) 164–172

Contents lists available at ScienceDirect

Chemical Engineering Journal

journal homepage: www.elsevier.com/locate/cej

Hydrogenation of chloronitrobenzene to chloroaniline over Ni/TiO_2 catalysts prepared by sol–gel method

Jixiang Chen*, Na Yao, Rijie Wang, Jiyan Zhang

Tianjin Key Laboratory of Applied Catalysis Science and Technology, Department of Catalysis Science and Engineering, School of Chemical Engineering and Technology, Tianjin University, Tianjin 300072, China

ARTICLE INFO

Article history:
Received 17 June 2008
Received in revised form
26 November 2008
Accepted 28 November 2008

Keywords:
Nickel catalyst
Sol–gel
Hydrogenation
Chloronitrobenzene
Chloroaniline

ABSTRACT

Ni/TiO_2 catalysts were prepared by the sol–gel method, and the effect of calcination and reduction temperatures on their physicochemical properties was investigated. The increase of the calcination temperature decreases the surface area and enhances the interaction between nickel species and support, which results in the decrease of the available nickel active sites and the catalyst performance. With raising the reduction temperature, the catalyst performance also declines due to the enhanced interaction between the nickel species and TiO*x* and the serious sintering of metallic nickel crystallites. The suitable calcination and reduction temperatures are 673 and 623 K, respectively. Under 348 K and 1.0 MPa, *o*-chloronitrobenzene conversion and *o*-chloroaniline selectivity over the optimum Ni/TiO_2 catalyst exceed 99%; moreover, the catalyst was not deactivated during 9 times recycles. The reasons for the catalyst deactivation were also investigated. It has been found that the main reason is the surface coverage and the pore blockage with bulky molecular species rather than the sintering of the metallic nickel crystallites. In addition, the hydrogenation activity of chloronitrobenzene (CNB) isomers decreases in the sequence of *m*-CNB, *o*-CNB and *p*-CNB. This sequence might be related to the electronic and steric factors of Cl substitute and the catalyst property.

1. Introduction

Aromatic chloroamines are important intermediates for the synthesis of many fine chemicals, such as dyes, drugs, herbicides, and pesticides. A main method for producing these haloamines is the reduction of the corresponding nitro-compounds, either with metal-acid or with hydrogen over a metal catalyst.

Catalytic hydrogenation is attractive and growing due to no acid effluents and little impact on environment. Many catalysts have been used for the hydrogenation of nitro-submitted aromatic chloro-compounds. These include polymer-stabilized colloidal noble metal clusters [1–5], supported noble metal catalysts [6–11], raney nickel [12], amorphous alloy [13–17], supported nickel catalysts [18–21], Co/C [22], and silica supported Ag [23] and Au [24] catalysts. The noble metal catalysts show a good catalytic performance even under mild reaction conditions, especially Pt catalysts; however, high cost and limited resource restrict their application. For raney nickel, there are some drawbacks in the industrial practice, such as the severe corrosion and pollution during its preparation and the safety problems during its storage and application. Moreover, in order to restrain dechlorination, some toxic promoters are used, and so the extra processing steps to remove them are necessary. Amorphous alloys show good activities, however, their thermal stability is essential to be improved. Supported nickel catalysts have been widely used in many hydrogenation reactions. Our previous works [18–20] show that TiO_2-supported nickel catalysts exhibit excellent performance in the hydrogenation of *o*-chloronitrobenzene (*o*-CNB) to *o*-chloroaniline (*o*-CAN). The conversion of *o*-CNB and the selectivity of *o*-CAN exceed 99% under the suitable conditions. Keane and co-workers [21] have reported that 100% selectivity of *p*-chloronitrobenzene to *p*-chloroaniline is obtained over the supported Ni catalysts in a fix-bed reactor under normal atmospheric pressure, offering a base for the development of a clean and high throughput production of commercially important haloamines. The above results indicate that the supported nickel catalysts are promising in the application.

The effect of transition metals on catalytic properties may be usually interpreted by geometric and/or electronic effects [25]. Coq et al. [6] has found that the hydrogenation rate of *p*-chloronitrobenzene increases as metallic Pt particles become larger in the Pt/Al_2O_3 catalysts, and attribute it to electronic-rich and multi-sites for adsorption on the larger particles. Chen and co-workers [13–15,17] suggest that the activity of the Ni-B and NiCoB nanometal catalysts is affected by the electronic structure of the metallic nickel, and indicate that the high electron density of Ni favors the hydrogenation of the nitro group. Zheng and co-workers

* Corresponding author. Tel.: +86 22 27890865; fax: +86 22 87894301.
E-mail address: jxchen@tju.edu.cn (J. Chen).

1385-8947/$ – see front matter © 2008 Elsevier B.V. All rights reserved.
doi:10.1016/j.cej.2008.11.046

[9,10] consider that electronic effect may play an important role in the good hydrogenation performance of Pt/ZrO_2 and Pt/TiO_2 catalysts modified by transition metals or rare earths. Electron deficient species of the second element promote the specific rate constant turnover frequency (TOF) by activating the nitrogen–oxygen bond. The supports also have a marked effect on the catalyst performance. As shown in the works from Coq et al. [11] and us [19], TiO_2 supported Pt or Ni catalyst shows better activity in comparison with SiO_2, MgO, and Al_2O_3 supported one. This is due to the strong interaction between the metal and the support. Ti*Ox* species produced during the reduction at high temperatures (above 573 K) can decorate metallic nickel particles [26,27]. Although they lead to the decrease of metallic nickel surface area, their oxygen vacancies could coordinate the oxygen atom in N=O group. As a result, N=O band is polarized and attacked easily by hydrogen atoms adsorbed on the nickel particles [19].

It is well known that the interaction between metal and TiO_2 can affect both catalytic activity and stability [28–30]. The interaction is related to some factors, such as preparation methods, and calcination and reduction conditions. In the previous work, it has been found that the activity of TiO_2 supported Ni catalyst increases with increasing nickel content due to increasing active surface [18]. When the nickel content exceeds 30 wt.%, the activity of the catalyst does not change remarkably. Moreover, there is an optimum calcination temperature of support for the catalysts prepared by the impregnation method [20], at which the catalyst has more nickel active sites and higher hydrogenation activity. Sol–gel method is an effective method for preparing highly dispersive catalysts [31]. It has been used to prepare supports and supported metal catalysts with high thermal stability, resistance to deactivation, and flexibility to control catalyst properties (such as particle size, surface area and pore size distribution). In order to prepare the catalysts with more active sites and optimum interaction between nickel and TiO_2, TiO_2 supported nickel catalyst was prepared by the sol–gel method in the present work. Since the calcination and reduction temperatures can influence the interaction between nickel and TiO_2, their effect on the properties of the catalysts was systematically investigated. The results show that the catalyst prepared the sol–gel method exhibits better performance than the impregnated one. In addition, the catalyst stability and the catalyst deactivation were investigated as well.

2. Experimental

2.1. Catalyst preparation

The catalysts were prepared by the sol–gel method. Firstly, two solutions were prepared, that is, tetrabutyl titanate was dissolved in ethanol, and $Ni(NO_3)_2{\cdot}6H_2O$ was dissolved in a mixture of ethanol and water. Secondly, the nickel nitrate solution was slowly added into the tetrabutyl titanate solution under the stirring, and a green transparent sol was obtained eventually. The sol was placed at the room temperature until a green gel formed. After the gel was dried at 383 K for 24 h, it was calcined at a temperature for 4 h, ranging from 473 to 823 K. The prepared catalysts are labeled as *SG*-T, where T denotes the calcination temperature. In the catalysts, the nickel mass content is about 17% measured by AAS.

As the reference, a catalyst was also prepared by the impregnation method according to the references [19,20]. The TiO_2 support (obtained from Nanjing High Technology Nano Co. Ltd., China) was impregnated with an aqueous solution of $Ni(NO_3)_2$ and left at room temperature for 12 h. After drying at 383 K for 4 h and calcination at 773 K for 4 h, the impregnated catalyst was prepared (labeled as *im*-Ni/TiO_2).

The reduced catalysts were passivated prior to some ex situ characterization, such as XRD and TG.

2.2. Catalyst characterization

Specific surface area and pore structure were measured with a Micromeritics TriStar 3 apparatus apparatus using N_2 adsorption and desorption at 77 K. The Brunauer-Emmett-Teller (BET) equation was used to calculate the specific surface area, S_{BET}. BET surface area was reproducible within ±5%. The Barrett-Joyner-Halenda (BJH) method applied over the desorption isotherm was used to determine the average pore diameter and the pore volume.

The Ni content in the catalyst was determined by AAS on a HITACHI 180-80 Polarized Zeeman Atomic Absorption Spectrophotometer. The analytic reproducibility was ±5%.

Hydrogen temperature-programmed reduction (H_2-TPR) was carried out in a tubular quartz reactor, into which a 40 mg catalyst was loaded. The reduction was conducted in a 10% H_2/N_2 flow at a heating rate of 10 K/min. Hydrogen consumption was determined using a thermal conduction detector (TCD) and its amount was quantified with CuO as reference.

X-ray diffraction (XRD) patterns were obtained on a PANalytical X'pert Pro diffractometer with Co Kα (λ = 0.17903 nm) radiation (40 kV, 40 mA). The average crystallite size was calculated using Scherrer equation.

The surface morphology of the catalyst was obtained by scanning electron microscopy (SEM) on a PHILIPS XL-30 ESEM.

Thermogravimetric analysis (TGA) and differential thermal analysis (DTA) were carried out with a Pyris Diamond TG/DTA instrument in an air flowing of 150 ml/min at a heating rate of 15 K/min.

Hydrogen chemisorption was measured on a TP-D/R/O 1100 SERIES (Finnigan) unit.

2.3. Catalyst activity test

Before the activity test, the catalyst was reduced at the designated temperature in 10% H_2/N_2 for 2 h. Liquid phase hydrogenation of CNB was carried out in a 250 ml stainless steel autoclave reactor, which was charged with CNB and the catalyst (CNB/catalyst mass ratio = 10) in ethanol. At first, air was flushed out of the reactor with nitrogen at room temperature, and hydrogen was then fed into the reactor. After replacing nitrogen with hydrogen, the reactor was heated to the designated temperature and pressure, and then the hydrogenation reaction started with stirring at 800 rpm. The experimental results show that the reaction was conducted in the absence of mass transfer limitation. During the run, a series of samples were withdrawn periodically and analyzed by a gas chromatograph equipped with a flame ionization detector (FID) and an OV-101 capillary column. The analytic reproducibility was better than ±1%. The products were identified by an Agilent GC6890-MS5973.

3. Result and discussion

3.1. Effect of calcination temperature on catalyst properties

3.1.1. Textural properties

Fig. 1 shows the N_2 adsorption isothermals of the catalysts calcined at different temperatures. All of the isothermals belong to IV types as defined by IUPAC [32]. The isotherm exhibits an inflection in p/p_0 range from 0.6 to 0.9, which is the characteristic of capillary condensation within the pores whose distribution and shape are not well-defined. The p/p_0 position of the inflection points is clearly related to a diameter in the mesopore range. The inset in Fig. 1 presents the pore size distribution. Table 1 shows the textural properties of the catalysts. With increasing the calcination temperatures, S_{BET} and pore volume of the catalysts decrease, while the

Table 1
Specific surface area, pore structure, H_2 chemisorption amount and H_2-TPR data of catalysts.

Catalyst	S_{BET} ($m^2\ g^{-1}$)	Pore volume, V_g ($cm^3\ g^{-1}$)	Average pore diameter (nm)	H_2 chemisorption (μmol/g cat)	H_2 consumption amount during H_2-TPR (mmol/g_{cat})	
					Theoretical value	Practical value
im-Ni/TiO_2[a]	84	0.193	9.2	1.5	–	–
SG-673	144	0.284	5.2	7.6	2.9	3.1
SG-723	111	0.263	6.2	8.5	2.9	3.1
SG-773	85	0.247	7.8	4.4	2.9	3.0
SG-823	51	0.195	10.6	2.1	2.9	3.0
Spent *SG*-673[b]	107	0.258	6.3	–	–	–

[a] Cited from reference [20].
[b] *SG*-673 catalyst recycled for 14 times.

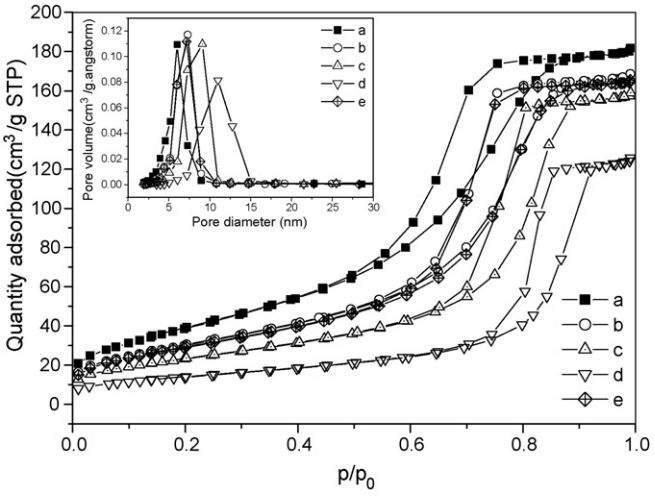

Fig. 1. N_2-adsorption isothermals and pore distributions of catalysts. (a) *SG*-673; (b) *SG*-723; (c) *SG*-773; (d) *SG*-823; (e) spent *SG*-673.

average pore diameter becomes larger and the pore distribution becomes broader. This is due to the catalyst sintering as shown by the XRD results (see Fig. 3).

3.1.2. TPR results

Fig. 2 shows the TPR profiles of the catalysts calcined at different temperatures. In the profile of *SG*-673, there is a main reduction peak (about 673 K) with a shoulder at lower temperature. For *SG*-723 and *SG*-773, only one reduction peak (about 700 K) is found. There are two reduction peaks at about 755 and 932 K in the reduction trace of *SG*-823. The reduction peak below 670 K can be attributed to the bulk NiO, the profile of which is shown in Fig. 2(a), while the peaks at the range of 670–755 K belong to NiO interacted with TiO_2 [33]. The reduction peak at about 932 K is attributed to $NiTiO_3$, which can be justified by the XRD results (see Fig. 3). It is clear that the reduction peaks shift to higher temperatures with increasing the calcination temperatures, indicating that the interaction between nickel species and TiO_2 becomes stronger. The practical H_2 consumption amount during the TPR was quantified with CuO as the reference, and the theoretical amount was corresponding to the requirement for Ni content in the catalyst. As shown in Table 1, the theoretical amount is slightly lower than the practical one, which is in the error range. This result indicates that there was no hydrogen spillover during H_2-TPR.

3.1.3. XRD and H_2 chemisorption results

Fig. 3 shows the XRD patterns of the catalysts in oxidation state. Apart from anatase TiO_2, there are only NiO phase in *SG*-673, *SG*-723, and *SG*-773. For *SG*-823, $NiTiO_3$ phase forms due to high calcination temperature. With increasing the calcination temperatures, the diffraction peaks of anatase TiO_2 and NiO become sharper, indicating there is a sintering of anatase TiO_2 and NiO crystallites. Based on TiO_2(200) and calculated with Scherrer equation, the anatase TiO_2 crystallite sizes in *SG*-673, *SG*-723, *SG*-773 and *SG*-823 are about 6, 8, 9 and 15 nm, respectively. The sintering of

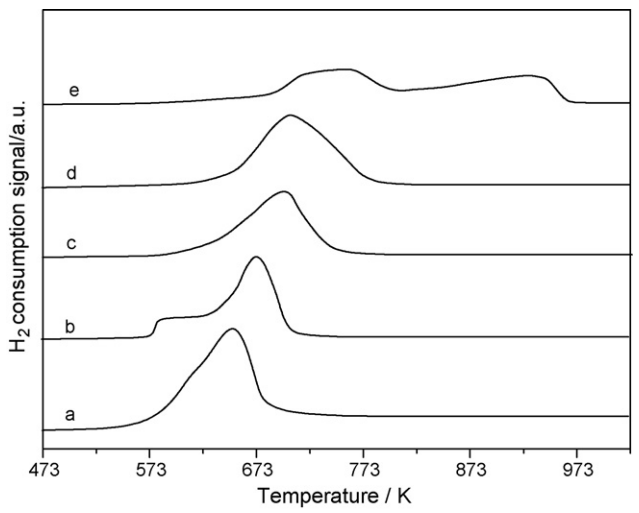

Fig. 2. H_2-TPR profiles of NiO and Ni/TiO_2 catalysts calcined at different temperatures. (a) NiO; (b) *SG*-673; (c) *SG*-723; (d) *SG*-773; (e) *SG*-823.

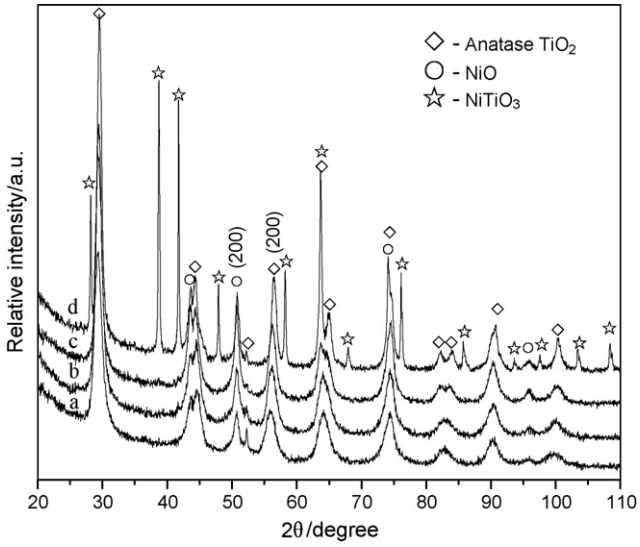

Fig. 3. XRD patterns of catalysts in oxidation state. (a) *SG*-673; (b) *SG*-723; (c) *SG*-773; (d) *SG*-823.

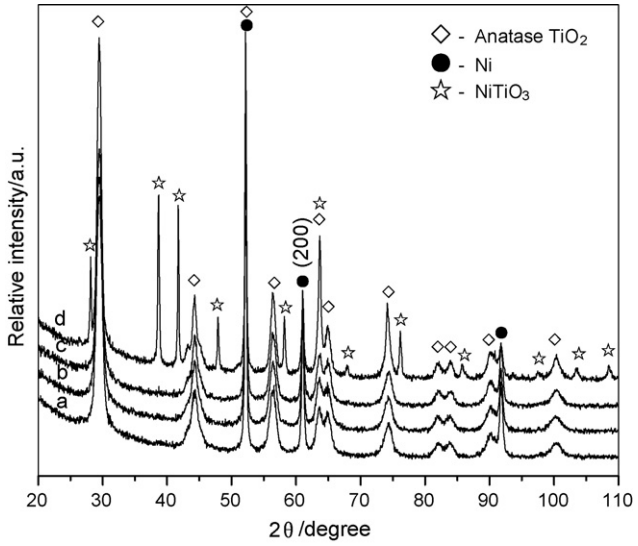

Fig. 4. XRD patterns of Ni/TiO2 catalysts reduced at 723 K. (a) *SG*-673; (b) *SG*-723; (c) *SG*-773; (d) *SG*-823.

anatase TiO_2 and NiO crystallites leads to low specific surface area and pore volume, and large pore diameter.

Fig. 4 shows the XRD patterns of the catalysts reduced at 723 K. For the catalysts calcined below 773 K, only Ni phase is detected except the support. This indicates that NiO is completely reduced at 723 K. for *SG*-823, $NiTiO_3$ is not reduced, which is consistent with TPR result. Based on Ni (200) and calculated with Scherrer equation, the nickel crystallite sizes in *SG*-673, *SG*-723, and *SG*-773 are all about 34 nm, whereas that in *SG*-823 is about 26 nm. It is well known that TiO_2 can be reduced to TiO*x* ($x<2$) species and this species can decorate the nickel crystallites. The decorating effect may restrain the nickel sintering, which can account for the similar metallic nickel crystallites for *SG*-673, *SG*-723, and *SG*-773. *SG*-823 has a smaller Ni crystallites size, which may be attributed to less amount reduced nickel species.

Table 1 shows H_2 chemisorption amounts of the catalysts. There is a trend that H_2 chemisorption amount decreases with increasing in the calcination temperature. This is related to the increased interaction between nickel species and the support. The strong interaction favors the decoration of TiO*x* on the metallic nickel crystallites and results in the decrease of the metallic active surface.

3.1.4. Catalyst performance

Fig. 5 shows the performance of the catalysts in the hydrogenation of *o*-CNB. Compared with the catalyst prepared by the impregnation method (*im*-Ni/TiO_2), the catalysts prepared *via* sol–gel method possess better activity, especially the ones calcined at lower temperatures. Over *SG*-673, *o*-CNB conversion and *o*-CAN selectivity exceed 99% after reaction for 90 min. *SG*-723 and *SG*-773 have similar performance, and *o*-CNB conversion and *o*-CAN selectivity over them exceed 97% and 99% after reaction for 120 min, respectively. *SG*-823 has a inferior performance, over which *o*-CNB conversion and *o*-CAN selectivity are about 31% and 88% after reaction for 210 min, respectively. During the first 60 min, the average hydrogenation TOFs over *SG*-673, *SG*-723, *SG*-773 and *SG*-823 are 2.3, 0.9, 1.2 and 0.3 s^{-1}, respectively. With increasing the calcination temperature of the catalyst, the hydrogenation TOF decreases. This indicates that there is a proper interaction between nickel species and the support for the hydrogenation, and too strong interaction is not favorable.

The hydrogenation of *o*-CNB is a multistep process as shown in Scheme 1 [34], and there are some intermediates in the reaction process. However, these intermediates can be converted to *o*-CAN. In the present study, some intermediates were found during the reaction with GC-MS. These include *o*-chloronitrosobenzene, *o*-chlorophenylhydroxylamine, and azodichlorobenzene. Among them, *o*-chloronitrosobenzene was the main intermediate during the reaction. Fig. 5(c) shows that the selectivity of *o*-chloronitrosobenzene decreases along with the reaction time.

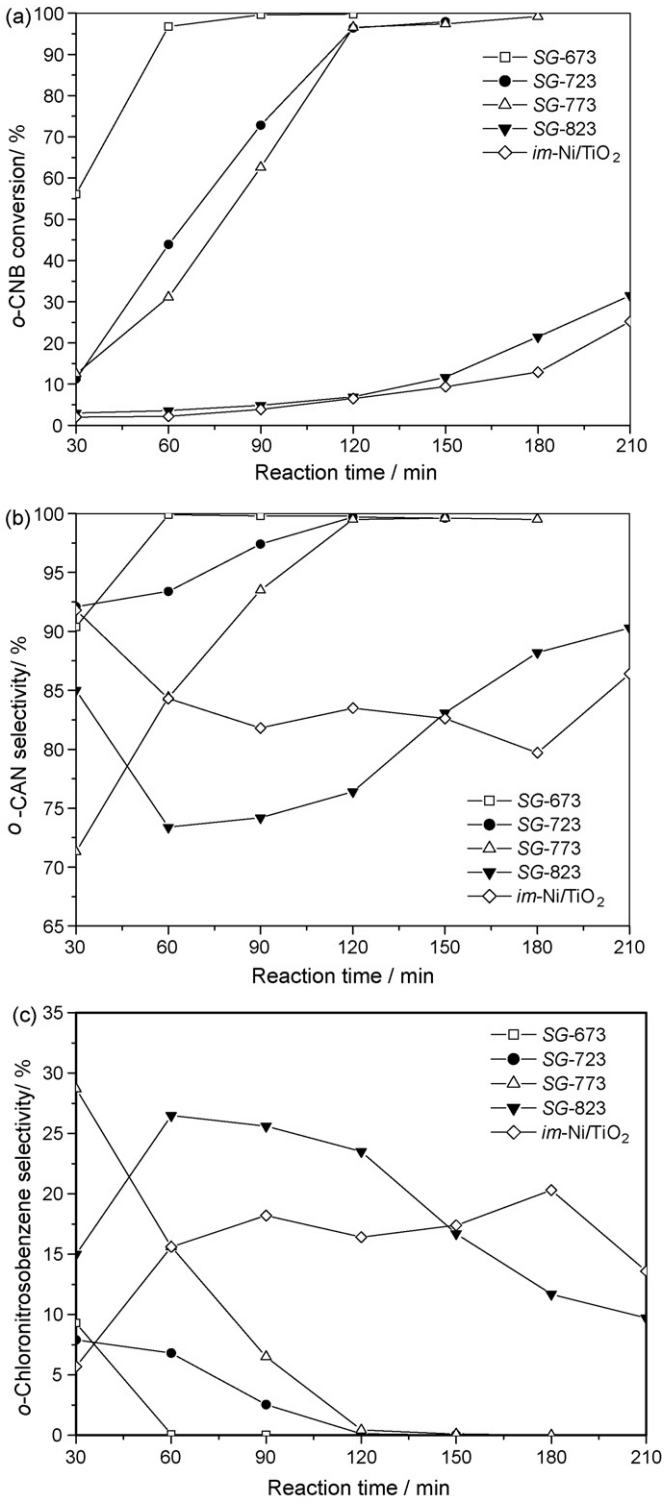

Fig. 5. Performance of catalysts in hydrogenation of *o*-CNB. (a) *o*-CNB conversion; (b) *o*-CAN selectivity; (c) *o*-chloronitrosobenzene selectivity. *Reaction conditions*: 348 K, H_2 1.0 MPa, 0.5 g catalyst, 5.0 g *o*-CNB, 120 ml ethanol.

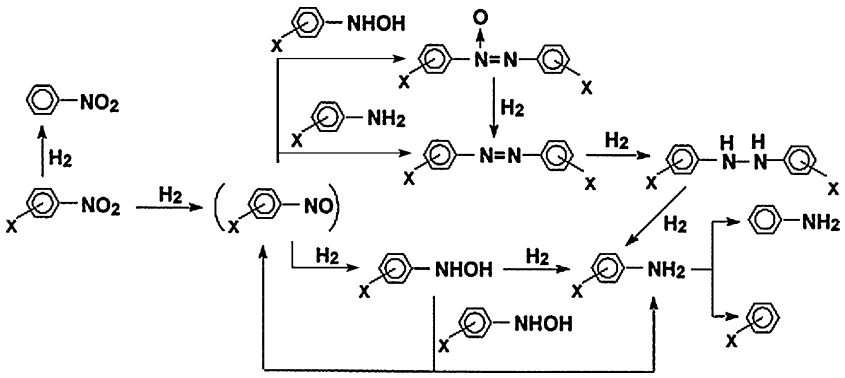

Scheme 1. Reaction scheme of CNB hydrogenation [34].

When the conversion of *o*-CNB exceeds 99%, the selectivity to *o*-CAN exceeds 99% and aniline becomes the main by-product due to hydrodechlorination.

Among the prepared catalysts, *SG*-673 exhibits the best performance. This is due to its more available active sites and the proper interaction between the nickel species and the support.

3.2. Effect of reduction temperature on catalyst properties

3.2.1. XRD results

Fig. 6 shows the XRD patterns of *SG*-673 catalyst reduced at different temperatures. Obtained from Fig. 6(b), NiO cannot be completely reduced at 573 K, and it is completely reduced to Ni above 623 K. With increasing the reduction temperature, the diffraction peaks of metal nickel become sharper, indicating the sintering of the nickel crystallites. Calculated with Scherrer equation based on the reflection of Ni(2 0 0), the nickel crystallite sizes are calculated as 14, 21, 27, 34 and 43 nm for *SG*-673 reduced at 573, 623, 673, 723 and 773 K, respectively.

3.2.2. Catalyst performance

Fig. 7 shows the performance of *SG*-673 reduced at the different temperatures in the hydrogenation of *o*-CNB. After reaction for 90 min, *o*-CNB conversion and *o*-CAN selectivity exceed 99% over *SG*-673 reduced between 623 and 723 K. *SG*-673 reduced at 573 K or 773 K has an inferior performance. When *SG*-673 was reduced at 573 K, the incomplete reduction of NiO (see Fig. 6(b)) leads to fewer active sites and so lower activity. When SG-673 was reduced at 773 K, the sintering of the metallic nickel crystallites become serious; meanwhile, the interaction between nickel and TiO*x* ($x < 2$) become stronger. It is well known that TiO*x* species produced during the reduction can decorate the nickel crystallites, which can decrease the available nickel surface by site-blocking. Moreover, the higher the reduction temperature is, the more remarkable the effect of the decoration. Raupp and Dumesic [35] have reported that the nickel surface decreases sharply when the reduction temperature exceeds 770 K. In the previous study [19], it is suggested

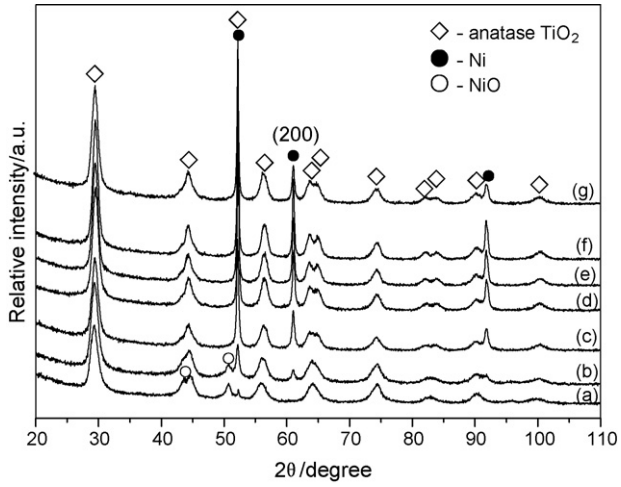

Fig. 6. XRD patterns of *SG*-673. (a) Unreduced and reduced at (b) 573 K; (c) 623 K; (d) 673 K; (e) 723 K; (f) 773 K; (g) spent *SG*-673 reduced at 623 K.

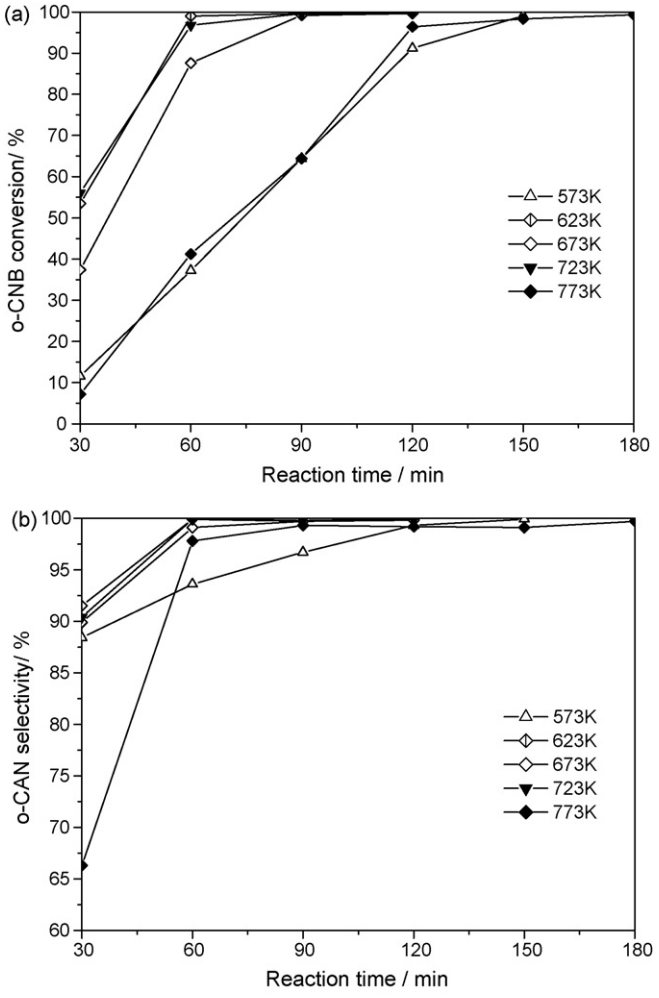

Fig. 7. Performance of *SG*-673 reduced at different temperatures. (a) *o*-CNB conversion; (b) *o*-CAN selectivity. *Reaction conditions*: 348 K, H_2 1.0 MPa, 0.5 g catalyst, 5.0 g *o*-CNB, 120 ml ethanol.

that there is a promotion effect of TiO*x* species in the hydrogenation of *o*-CNB. The oxygen vacancy of TiO*x* can coordinate the oxygen atom in N=O group. As a result, N=O band is polarized and attacked easily by hydrogen atoms adsorbed on the nickel particles. This synergism between Ni and TiO*x* promotes the hydrogenation of *o*-CNB. However, higher reduction temperature can promote the sintering of nickel crystallites and the decoration of TiO*x*, all of which lead the decrease of the active sites.

3.3. Hydrogenation of different CNB isomers

Fig. 8 shows the performance of *SG*-673 in the hydrogenation of different CNB isomers. *SG*-673 was reduced at 623 K prior to the test. According to the first 30 min, the reactivity of CNB decreases in the order: *m*-CNB > *p*-CNB > *o*-CNB. Although *p*-CNB conversion is slightly lower than that of *o*-CNB and *m*-CNB, it exceeds 98% after reaction for 120 min, and *p*-CAN selectivity is above 99%. For the hydrogenations of *o*-CNB and *m*-CNB, all of the conversion and the selectivity exceed 99% after reaction for 60 min. It is obvious that *SG*-673 is a good catalyst in the hydrogenation of the different CNB isomers.

It has been known [36,37] that the rate determining step of the hydrogenation of nitrobenzene derivatives is a nucleophilic attack of hydride ion, produced by dissociative adsorption of H_2 molecule on the metal surface, on the nitrogen atom of the nitro group. Therefore, electron withdrawing and electron donating effects of the substituents may have a strong influence on the reactivity of CNB isomers. It has been suggest that the hydrogenation of nitrobenzene derivatives is aided by the electron withdrawal from the benzene ring. The difference in the reactivity of CNB partially corresponds to the Hammett constants of chloro-substituent in *m*-CNB and *p*-CNB, which are 0.37 and 0.24, respectively [37]. The influence of *o*-CNB is not possible to explain via the Hammett constant, because –Cl and $–NO_2$ groups in ortho position are in mutual interaction. There is a steric effect between –Cl and NO_2 in *o*-CNB, which is not favorable to the hydrogenation. Apart from the effect of substituent, the catalyst properties (including electronic and geometrical aspects) also influence the hydrogenation rate of different CNB isomers. Kralik and co-workers [37] report that an anionic polymer supported Pd catalyst corresponding to maximum catalytic activity vary in the following order: *m*-CNB > *p*-CNB > *o*-CNB; however, the hydrogenation rates of CNB over the charcoal-supported Pd catalyst vary in the sequence: *p*-CNB > *o*-CNB > *m*-CNB. Over the Pt/TiO_2 and Pt/ZrO_2 catalysts, the rates of the hydrogenation decrease in the order of *m*-CNB, *p*-CNB and *o*-CNB [9,10].

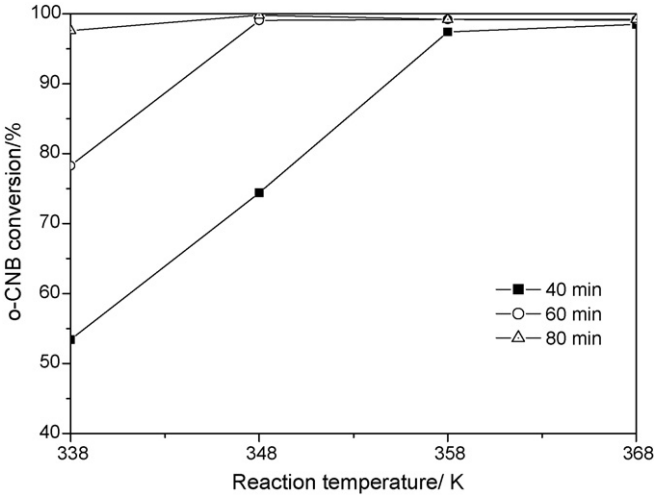

Fig. 9. Effect of reaction temperature on hydrogenation of *o*-CNB. *Reaction conditions*: H_2 1.0 MPa, 0.5 g catalyst, 5.0 g *o*-CNB, 120 ml ethanol.

3.4. Effect of reaction conditions on hydrogenation of o-CNB

o-CNB was selected as the reactant, and the effect of reaction conditions on its hydrogenation was carried out over the *SG*-673 catalyst reduced at 623 K.

3.4.1. Effect of reaction temperature

Effect of reaction temperature on the hydrogenation of *o*-CNB is illustrated in Fig. 9. With the rise of the reaction temperature, all of *o*-CNB conversion and *o*-CAN selectivity increase. When the temperature is 348 K, *o*-CNB conversion and *o*-CAN selectivity exceed 99% after reaction for 60 min.

3.4.2. Effect of H_2 pressure

Fig. 10 shows the effect of H_2 pressure on the hydrogenation of *o*-CNB. With increasing H_2 pressure, *o*-CNB conversion increases. After reaction for 60 min, the effect of H_2 pressure on the hydrogenation of *o*-CNB is not remarkable when H_2 pressure exceeds

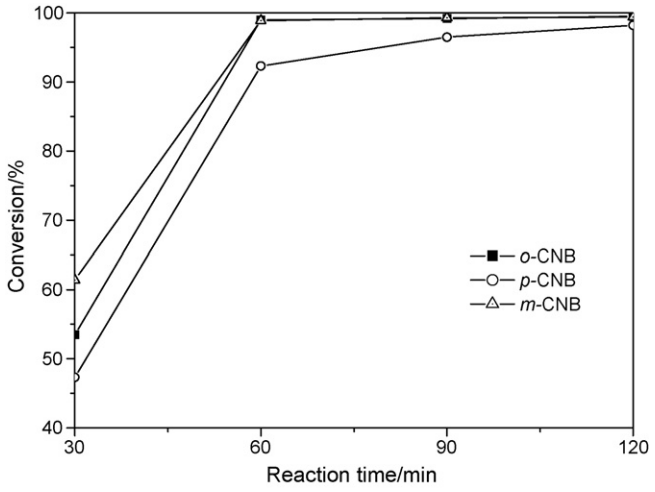

Fig. 8. Performance of *SG*-673 in hydrogenation of different CNB isomers. *Reaction conditions*: 348 K, H_2 1.0 MPa, 0.5 g catalyst, 5.0 g CNB, 120 ml ethanol.

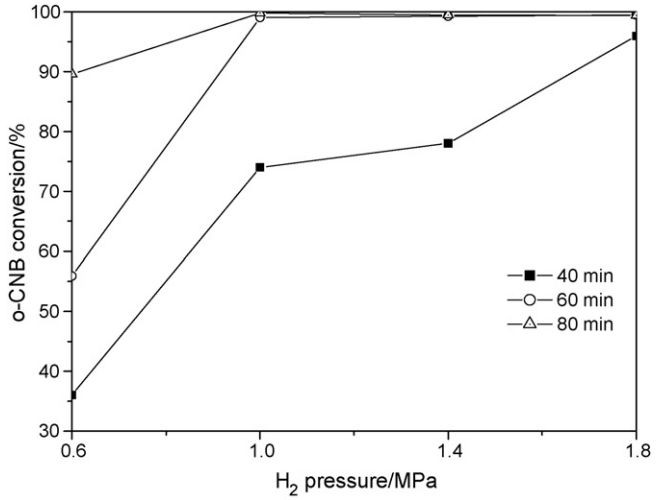

Fig. 10. Effect of H_2 pressure on hydrogenation of *o*-CNB. *Reaction conditions*: 348 K, 0.5 g catalyst, 5.0 g *o*-CNB, ethanol 120 ml.

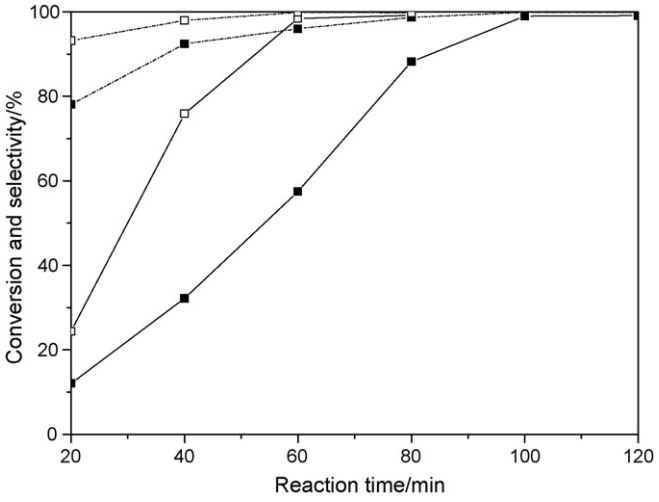

Fig. 11. Effect of catalyst/*o*-CNB mass ratios (□: 0.1; ■: 0.05) on hydrogenation of *o*-CNB; solid lines corresponding to *o*-CNB conversion, dashed corresponding to *o*-CAN selectivity. *Reaction conditions*: 348 K, H_2 1.0 MPa, 0.5 g catalyst, 120 ml ethanol.

1.0 MPa. In this case, all of *o*-CNB conversion and *o*-CAN selectivity are above 99%.

3.4.3. Effect of catalyst/o-CNB mass ratio

Fig. 11 shows the effect of mass ratio of the catalyst and *o*-CNB on the hydrogenation of *o*-CNB. As the decrease of the catalyst/*o*-CNB mass ratio, it takes longer time that *o*-CNB conversion and the *o*-CAN selectivity reach 99%.

3.5. Catalyst stability and deactivation

3.5.1. Catalyst stability

SG-673 catalyst reduced at 623 K was selected to investigate the catalyst stability. During the recycle of the catalyst, no fresh catalyst was added. After each reaction, the catalyst was firstly subsided for some time, and the solution was slowly withdrawn. During the whole test process, the catalyst was always stored carefully in the ethanol and the solution, avoiding to be oxidized by air.

Fig. 12 shows the catalyst performance during the recycles. The reaction time in each recycle was fixed as 60 min. In the first 9 recycles, *o*-CNB conversion and *o*-CAN selectivity were above 99%. When the catalyst was further recycled, its performance declined, that is, the catalyst was deactivated. In the thirteenth recycle, *o*-CNB conversion was only about 85%, and *o*-CAN selectivity was 98%. Before the fourth recycle, the catalyst was washed with ethanol for 3 times. The performance of the washed catalyst did not decrease further in comparison with the thirteenth recycle, but it was also lower than that of the fresh catalyst. This indicates that the washing with ethanol only partially regenerated the catalyst.

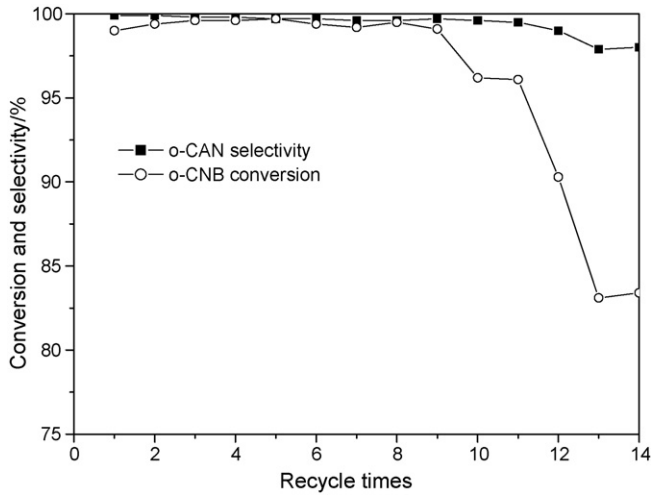

Fig. 12. Result of catalyst stability. *Reaction conditions*: 348 K, H_2 1.0 MPa, 0.8 g catalyst, 8.0 g *o*-CNB, 120 ml ethanol, reaction time of each run 60 min.

3.5.2. Catalyst deactivation analysis

In order to investigate the reasons for the catalyst deactivation, the spent catalyst (that is, spent *SG*-673) used for 14 times was characterized, and the result is compared with that of the fresh catalyst.

Compared with the fresh catalyst, the specific surface area and the pore volume of the spent one decrease, while the pore diameter of the spent one becomes wider (see Fig. 1 and Table 1). This may be due to the surface coverage and the pore blockage with the bulky molecular species formed during the reaction. The bulky molecular species deposited on the spent catalyst can be tested by TG method. Fig. 13 shows the TG and DTA curves of the fresh and the spent catalysts. From room temperature to about 490 K, there are mass-losses in the TG curves of the two samples, which is owing to the desorption of the adsorbed water. For the fresh sample, there is a 3.5% mass-increase from 490 to 700 K due to the oxidation of metallic nickel; synchronously, there is a remarkable exothermic peak in the DTA curve. However, for the spent sample, there is a mass-loss of 0.4% in the TG curve and a exothermic peak in the DTA

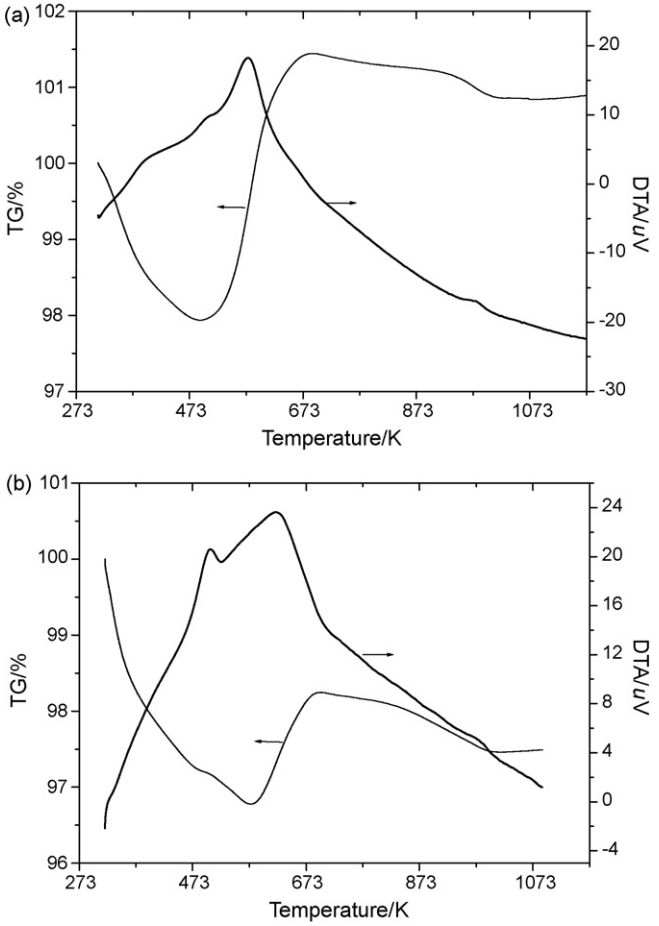

Fig. 13. TG/DTA curves of (a) fresh *SG*-673 catalyst and (b) spent *SG*-673 catalyst.

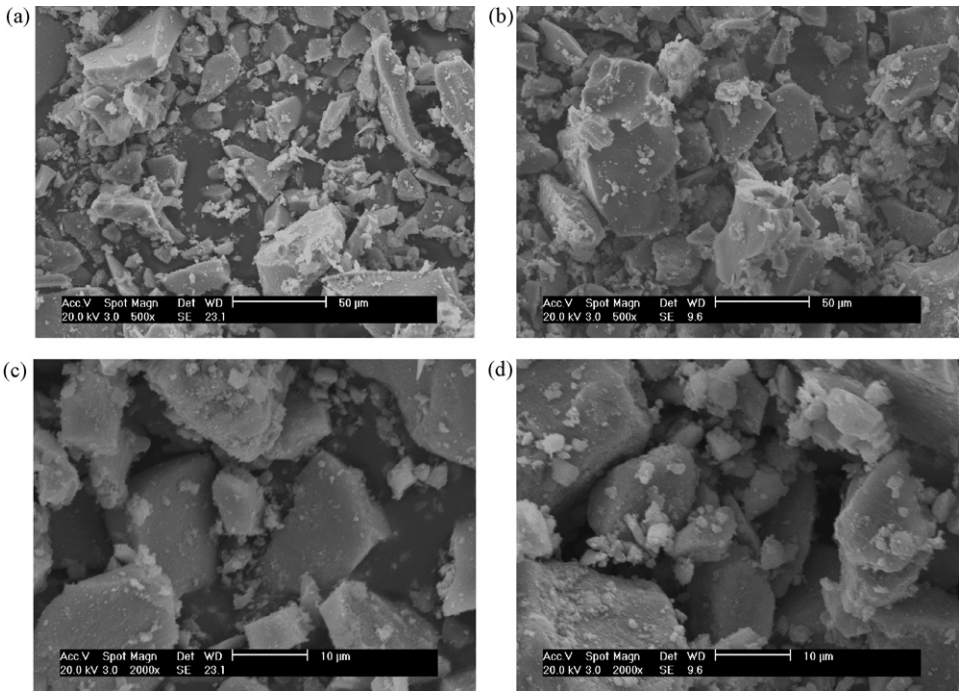

Fig. 14. SEM micrographs of fresh catalyst (a, c) and spent catalyst (b, d).

curve from 490 to 570 K, which are attributed to the oxidation of the adsorbed organic substance; afterward, a 1.5% mass-increase stage and an exothermic process from 570 to 700 K are attributed to the oxidation of metallic nickel. In comparison with the fresh sample, it is clear the mass-increase due to the oxidation of metallic nickel is less for the spent sample. This phenomenon may be related to the oxidation of the adsorbed organic substance in the spent sample, which masks the mass-increase due to the oxidation of metallic nickel. Above 700 K, a mass-decrease occurs in the TG curves of the both samples. This may be related to the oxidation of the carbonaceous residues derived from the preparation process [38], which can be reflected by the exothermic peak (at about 973 K) in the DTA curves. The above results indicate that there are the adsorbed bulky molecular species in the spent catalyst, resulting from the polymerization or/and condensation of reactant and/or product during the reaction. As shown in Scheme 1, the hydrogenation of chloronitrobenzene is a multi-step process, and there are some larger intermediate molecules produced during the reaction. Though these molecules can be converted to chloroaniline eventually, they may adsorb on the catalyst surface easily and then block the pores; moreover, they also can polymerize or/and condense to form more lager intermediates. These larger intermediates would adsorb on the surface, block the pores (especially micropores) and cover the metal nickel, in turn, leading to the catalyst deactivation.

As shown in Fig. 6(c) and (g), there is no remarkable difference in XRD patterns between the fresh catalyst and the spent one. Based on the reflection of Ni(2 0 0) and calculated with Scherrer equation, the nickel crystallite sizes in the fresh catalyst and the spent one are 21 and 22 nm, respectively. This indicates that the catalyst deactivation is not derived from the metallic nickel sintering. In addition, as shown in SEM micrographs (Fig. 14), there is no remarkable difference in the size and the surface of the catalyst particles between the fresh catalyst and the spent one.

According to the above results, it is suggested that the surface coverage and the pore blockage of bulky molecular species is the important reason for the catalyst deactivation.

4. Conclusions

Ni/TiO_2 catalyst was prepared by the sol–gel method. There is a remarkable effect of the calcination and reduction temperatures on the catalyst properties. The increase of the calcination temperature results in the decrease of the specific surface area and the pore volume, and the increase of the pore diameter; meanwhile, the interaction between nickel species and TiO*x* increases. The decrease of specific surface area and the enhancement of the interaction between nickel species and TiO*x* lead to the decrease of the available nickel active sites. In turn, the catalyst performance decreases. With raising the reduction temperature, the interaction between the nickel species and TiO*x* is also enhanced, and the sintering of nickel crystallites becomes serious. All of these also make the catalyst performance decrease. The catalyst calcined at 673 K and reduced at 623 K showed excellent performance in the hydrogenation of *o*-, *m*- and *p*-chloronitrobenzene. Over it, *o*-CNB conversion and *o*-CAN selectivity exceeded 99% after reaction for 60 min at 348 K and 1.0 MPa. The catalyst recycled for 9 times was not deactivated and the deactivation took place at the tenth recycle. The characterization results show that the main reason for the catalyst deactivation is attributed to the surface coverage and the pore blockage with bulky molecular species.

Acknowledgements

This work was supported by the Natural Science Foundation of Tianjin (No. 08JCYBJC01600) and the Program of Introducing Talents to the University Disciplines (No. B06006).

References

[1] W.X. Tu, H.F. Liu, Y. Tang, J. Mol. Catal. A: Chem. 15 (2000) 115.
[2] X.P. Yan, M.H. Liu, H.F. Liu, K.Y. Liew, N. Zhao, J. Mol. Catal. A: Chem. 170 (2001) 203.
[3] X.X. Han, R.X. Zhou, G.H. Lai, B.H. Yue, X.M. Zheng, React. Kinet. Catal. Lett. 81 (2004) 41.
[4] S.G. Xu, X.L. Xi, J. Shi, S.K. Cao, J. Mol. Catal. A: Chem. 160 (2000) 287.
[5] Z.K. Yu, S.J. Liao, Y. Xu, B. Yang, D.R. Yu, J. Mol. Catal. A: Chem. 120 (1997) 247.

[6] B. Coq, A. Tijani, F. Figueras, J. Mol. Catal. 68 (1991) 331.
[7] W.Y. Yu, H.F. Liu, X.H. An, X.M. Ma, Z.J. Liu, L. Qiang, J. Mol. Catal. 147 (1992) 73.
[8] B.J. Zuo, Y. Wang, Q.L. Wang, J.L. Zhang, N.Z. Wu, L.D. Peng, L.L. Gui, X.D. Wang, R.M. Wang, D.P. Yu, J. Catal. 222 (2004) 493.
[9] X.X. Han, R.X. Zhou, G.H. Lai, B.H. Yue, X.M. Zheng, J. Mol. Catal. A: Chem. 209 (2004) 83–87.
[10] X.X. Han, R.X. Zhou, G.H. Lai, B.H. Yue, X.M. Zheng, Catal. Lett. 89 (2003) 255.
[11] B. Coq, A. Tijani, R. Dutartre, F. Figuéras, J. Mol. Catal. 79 (1993) 253.
[12] R.J. Maleski, E.T. Mullins, US 6034276.
[13] Y.C. Liu, C.Y. Huang, Y.W. Chen, J. Nanopart. Res. 8 (2006) 223–234.
[14] Y.C. Liu, Y.W. Chen, Ind. Eng. Chem. Res. 45 (2006) 2973–2980.
[15] L.F. Chen, Y.W. Chen, Ind. Eng. Chem. Res. 45 (2006) 8866–8873.
[16] X.H. Yan, J.Q. Sun, Y.W. Wang, J.F. Yang, J. Mol. Catal. A: Chem. 252 (2006) 17–22.
[17] J.H. Shen, Y.-W. Chen, J. Mol. Catal. A: Chem. 273 (2007) 265–276.
[18] J. Xiong, J.X. Chen, J.Y. Zhang, Chin. J. Catal. 27 (2007) 579.
[19] J. Xiong, J.X. Chen, J.Y. Zhang, Catal. Commun. 8 (2007) 345.
[20] N. Yao, J.X. Chen, J.X. Zhang, J.Y. Zhang, Catal. Commun. 9 (2008) 1510–1516.
[21] F. Cárdenas-Lizana, S. Gómez-Quero, M.A. Keane, Appl. Catal. A 334 (2008) 199–206.
[22] L. Xing, J.S. Qiu, C.H. Liang, C. Wang, L. Mao, J. Catal. 250 (2007) 369–372.
[23] Y.Y. Chen, C. Wang, H.Y. Liu, J.S. Qiu, X.H. Bao, Chem. Commun. 42 (2005) 5298–5300.
[24] Y.Y. Chen, J.S. Qiu, X.K. Wang, J.H. Xiu, J. Catal. 242 (2006) 227–230.
[25] B. Coq., F. Figueras, Coordin. Chem. Rev. 178–180 (1998) 1753–1783.
[26] C. Hoang-van, Y. Kachaya, S.J. Teichner, Appl. Catal. A 46 (1989) 269.
[27] E. Ruckenstein, H.Y. Wang., J. Catal. 187 (1999) 151.
[28] A.M. Diskin, R.H. Cunningham, R.M. Ormerod, Catal. Today 46 (1998) 147.
[29] J.V. Loosdrecht, A.M.V. Kraan, A.J.V. Dillen, J.W. Geus, J. Catal. 170 (1997) 217.
[30] A. Dandekar, M.A. Vannice, J. Catal. 183 (1999) 344.
[31] R.D. Gonzalez, T. Lopez, R. Gomez, Catal. Today 35 (1997) 293–317.
[32] K.S.W. Sing, D.H. Everett, R.A.W. Haul, L. Moscow, R.A. Pierotti, J. Rouquerol, T. Siemieniewska, Pure Appl. Chem. 57 (1985) 603.
[33] S.W. Ho, C.Y. Chu, S.G. Chen, J. Catal. 178 (1998) 34.
[34] B. Coq, A. Tijani, F. Figueras, J. Mol. Catal. 71 (1992) 317.
[35] G.B. Raupp, J.A. Dumesic, J. Catal. 97 (1986) 85–99.
[36] P. Lu, N. Toshima, Bull. Soc. Jpn. 73 (2000) 751.
[37] V. Kratky, M. Kralik, M. Mecarova, M. Stolcova, L. Zalibera, M. Hronec, Appl. Catal. A 235 (2002) 225–231.
[38] D.P. He, F.R. Lin, Mater. Lett. 61 (2007) 3385–3387.